NPL
National Physical Laboratory

Report

NPL REPORT AS 24

Investigations relating to airborne nanoparticle sizing and number concentration

Richard J. J. Gilham

NOT RESTRICTED

May 2008

National Physical Laboratory | Hampton Road | Teddington | Middlesex | United Kingdom | TW11 0LW

Switchboard 020 8977 3222 | **NPL Helpline** 020 8943 6880 | **Fax** 020 8614 0446 | **www.npl.co.uk**

Department for **Innovation, Universities** & **Skills**

Investigations relating to airborne nanoparticle sizing and number concentration

Richard J. J. Gilham
Quality of Life Division

ABSTRACT

This report summarises investigations into various aspects of airborne nanoparticle instrumentation relating to Scanning Mobility Particle Sizers and Condensation Particle Counters, with a focus on the development and evaluation of a calibration procedure for Condensation Particle Counters.

The work was carried out within the National Measurement System's Chemical and Biological Metrology programme, project P1.

ISSN 1754-2928

National Physical Laboratory
Hampton Road, Teddington, Middlesex, TW11 0LW

Approved on behalf of the Managing Director, NPL
By Dr Neil Harrison, Group Leader, Analytical Science Team

Investigations relating to airborne nanoparticle sizing and number concentration

Table of Contents

1 Introduction

Nanoparticles, taken here to mean particles ranging in size from around 1 nm to around 1 μm, are of great current interest for both industrial and scientific reasons. Such particles are typically present in ambient air in concentrations of several thousand per cm^3, originating from natural processes (eg sea salt), combustion processes and nanotechnology industries. They play an important role in both health effects and climate change. Measurements of the size and number concentration of airborne nanoparticles are made for reasons of ambient monitoring, occupational exposure, cleanroom monitoring, vehicle/industrial emission monitoring, industrial process control, and fundamental aerosol science research.

Number concentration measurements are typically carried out using Condensation Particle Counters (CPCs) (also known as Particle Nucleation Counters). For size distributions, CPCs can be used in conjunction with Differential Mobility Analysers (DMAs), which indirectly sort the particles according to their aerodynamic diameter, by bringing them to an equilibrium charge distribution and selecting them by their electrical mobility. The combined CPC and DMA system is often referred to as a Scanning Mobility Particle Sizer (SMPS).

Calibration of such instruments simply for size is relatively straightforward through the use of aerosolised spheres whose diameter has been certified by TEM or other methods. Calibration of CPCs, or of SMPS size distributions, where much data processing is required to generate number concentrations as a function of size, have more complex metrological problems, and these have only recently received attention.

This report summarises investigations leading to a robust CPC calibration procedure, with related investigations into the effects of different charge distributions, detailed DMA performance and diluter characteristics.

2 Calibration of number concentration

The generally accepted means for calibrating CPCs is by comparison with a Faraday Cup Electrometer (FCE). Strictly speaking this is more of a validation by an independent method. In its ideal form, particle number concentration in an airstream containing only singly-charged particles is determined simultaneously by the CPC and by measuring the current carried by the particles. Through a calibration of the electrical assembly and the flow through the instrument, the charge density per unit volume of air can be determined. Unfortunately, this comparison is not trivial from a metrology point of view because there are many experimental variables that may affect the reference and test instruments differently. This section describes these variables such that a list of criteria for a calibration procedure can be compiled, which will be met in subsequent sections of this report.

In such a calibration experiment, the reference instrument (the FCE) and the test instrument (the CPC) simultaneously measure the number concentration of a test sample being produced by the aerosol generator. Any differences between the

measurands of each instrument need to be accounted for. To elucidate these differences, each instrument type is considered in turn.

2.1 Faraday Cup Electrometer

The FCE consists of three main components: the filter used to collect the aerosol, the electrometer and the pump. Ignoring transport losses, these are the main three components that affect the performance of the instrument. From this, we obtain our first criteria:

- The collection efficiency of the filter should be known.
- The electrometer must be calibrated.
- The flow must be measured using a calibrated flowmeter.

Although all particles have a finite probability of charging through collisions with ions in the air (or carrier gas), the sample will have an overall neutral charge and the electrometer will give a zero response unless steps are taken to prepare the sample such that particles of only one polarity are present. Furthermore, it is important to know the charge-state of the particles being measured to allow a charge concentration to be converted to a number concentration. This gives two more criteria:

- The particles sampled must all have the same polarity.
- The particles sampled must be singly charged or have a known charge distribution.

The measurement range of the electrometer must also be considered. Commercially available electrometers are capable of measuring currents of the order of a few femtoamps (fA). When combined with a typical flow rate, these instruments can provide measurements down to <1000 cm^{-3}. Electrometers of the type generally used saturate at concentrations comparable to those that can be measured by CPCs (>500,000 cm^{-3}). Therefore, we need only be concerned about the low concentration limit. Drift and instability in the number concentration of the test sample will also act to limit the lowest measurable concentration above the baseline noise of the electronics. These considerations give some more criteria:

- The minimum measurable concentration is at worst ~1000 cm^{-3}.
- Zero measurements are required to establish the baseline noise of the FCE.
- The test sample should be as stable as possible to obtain the best possible performance from the FCE.

2.2 Condensation Particle Counter

The requirements of the test instrument should also be considered to ensure that the probability of any calibration artefacts are minimised. A basic schematic of the CPC is shown in Figure 1. Ignoring transport losses, there are several factors that affect the instrument response, including the efficiency/capacity of the evaporator and condenser to enlarge the particles to a measurable size, the detection efficiency of the optical assembly given the outcome of the condensation process, the algorithm used to calculate the number concentration and the performance of the pump. These considerations yield a number of initial criteria:

- The sample should be chosen such that a nominal ~100% counting efficiency is achieved, or that else the sample used should be specific to the type that is to be routinely measured.
- The concentration range of the calibration must not exceed the capacity of the CPC to grow particles sufficiently.
- The calibration procedure should be sympathetic to the algorithm used by the CPC to calculate the number concentration.
- The flow must be measured using a calibrated flowmeter.

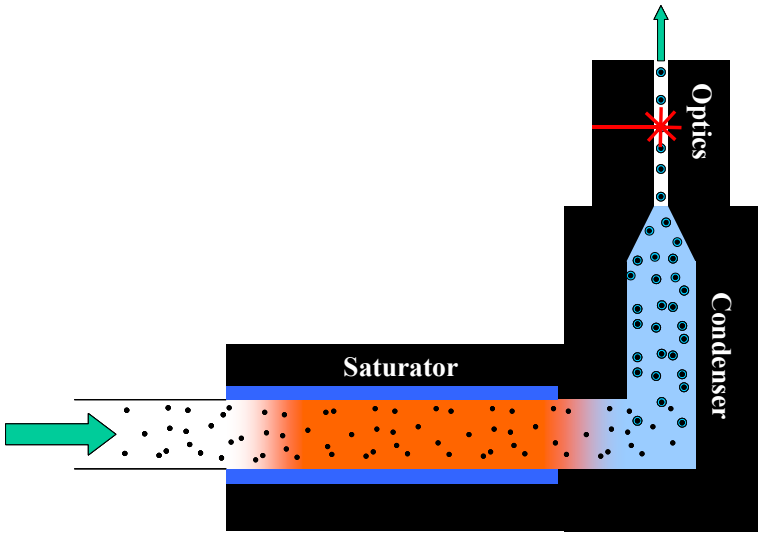

Figure 1: Basic schematic of the Condensation Particle Counter

Closer consideration of these criteria provides more information about what is required:

There is considerable debate as to the significance of material-dependent effects on the detection efficiencies of different CPC designs and this has yet to be resolved to the satisfaction of all stakeholders, particularly in the vehicle emissions area where there may be significant financial implications on the outcome. As such, care needs to be taken to ensure that the material used for the calibration is acceptable for this purpose and a suitable analogue for the particles to be measured by the customer afterwards. For example, the use of a hydrophobic particle material with a water-based CPC would be ill advised.

In addition to this, the detection efficiency of all CPCs decreases as the particle size is reduced. The particle size-dependent detection efficiency curves for a range of different CPC models are shown in Figure 2. From this it can clearly be seen that the calibration should be done with particles larger than 50 nm. There is also a special class of CPCs known as Particle Measurement Programme (PMP)-compliant CPCs, which have their performance modified to shift the efficiency drop-off to larger sizes to meet the requirements of the PMP regulations. The calibration procedures associated with these instruments require calibration to be carried out with particles between 50 and 100 nm.

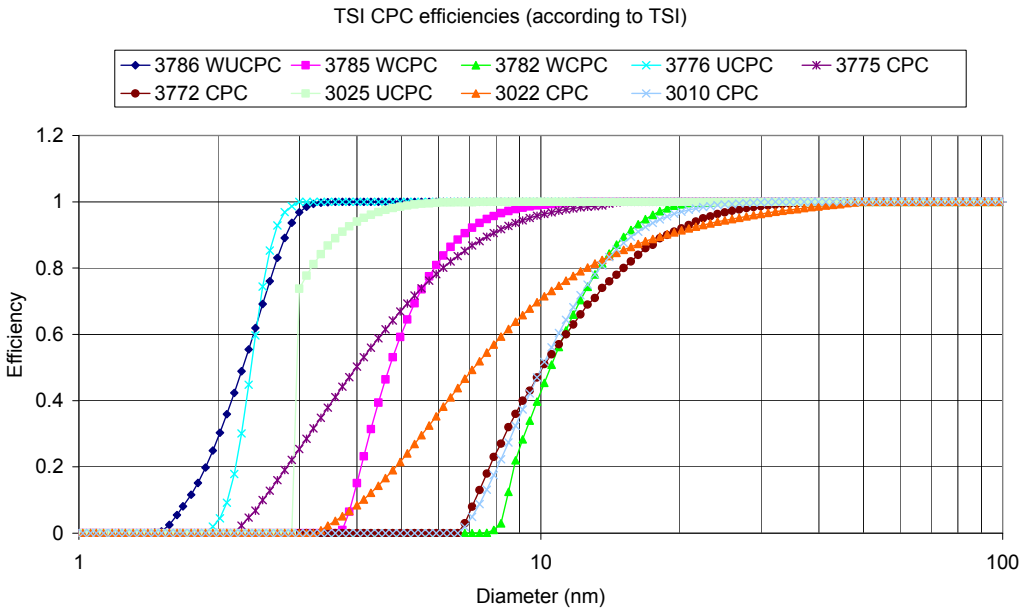

Figure 2: Typical CPC size-dependent detection efficiency curves.

The concentration ranges over which different models of CPC operate vary. In general, there are three different general designs that need to be considered. The first are regular design, single particle counting CPCs. These are the simplest design and can often only measure concentrations up to 10 000 cm^{-3}. The second are ultrafine CPCs. These instruments also only generally use a single counting mode, but can measure much higher concentrations due to an internal dilution mechanism. Finally, multimode CPCs, which utilise both single particle counting, usually up to 10 000 cm^{-3}, and an empirical photometric mode at higher concentrations. Therefore, the concentration range of the calibration must be chosen with care.

2.3 Other Considerations

In addition to the above criteria, the calibration experiment should be designed to minimise other sources of error. The major remaining considerations are the effect of differing transport losses in the lines delivering the sample to the instruments, and the effect of uncharged or multiply charged particles in the airstream to the instruments. There is no need to determine the absolute magnitude of the losses in each line, but rather minimise any differences such that they are only a small contributor to the overall experimental error. This gives our final criteria:

- The sample delivered to the inlet of both instruments should be equivalent;
- Effects of non-singly charged particles need to be assessed and, if necessary, accounted for.

2.4 CPC Calibration Procedure

From the previous section, a number of criteria for the calibration procedure have been elucidated. The procedure described here has been designed to meet these criteria.

2.4.1 Experimental design

The experimental section of the calibration consists of two parts. In the first, data for applying a correction to account for multiply charged particles is collected, and in the second, the calibration data itself is recorded. Throughout the experimental section, care is taken to account for drift in the zero point of the electrometer and the output of the particle generator. This lengthens the experiment significantly, but yields superior quality data. The collection of the data is driven by a data analysis spreadsheet.

Although the general procedure is identical for all types of test particles, there is some variation in the practicalities for different particle types. In the first instance the procedure was optimised for measuring soot particles generated by the CAST2 soot generator manufactured by Matter Engineering. This variation will be taken as a case study to demonstrate the performance of the procedure. The general block diagram for the experimental configuration is shown in Figure 3.

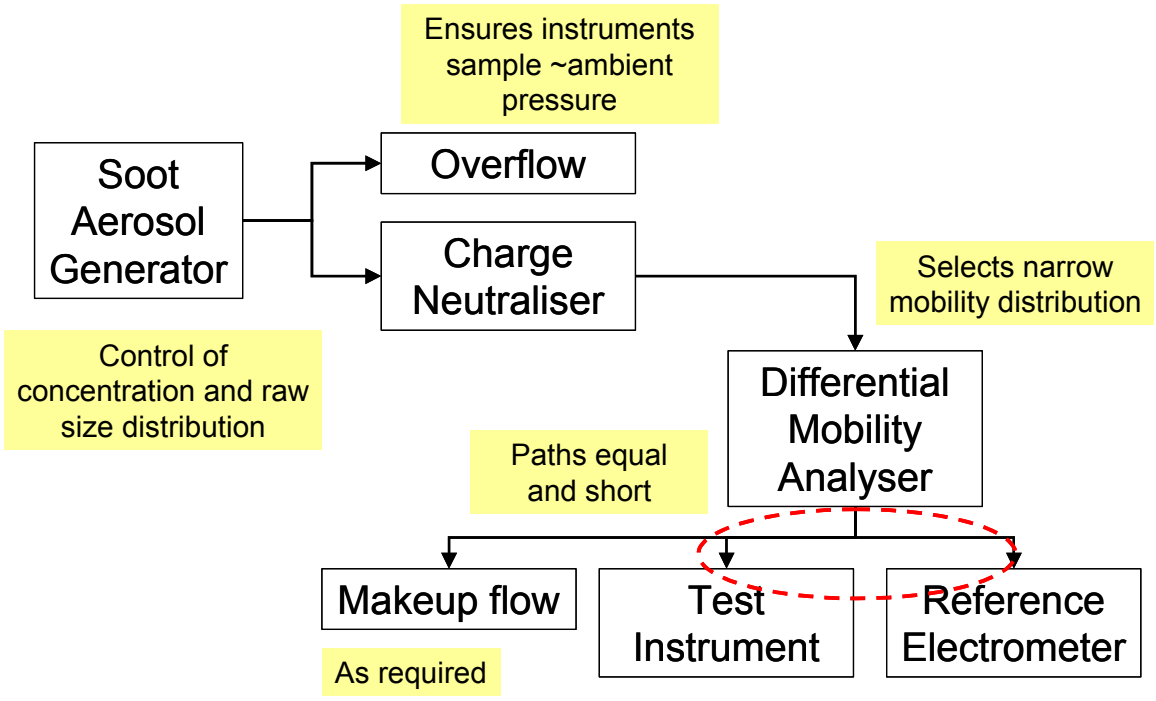

Figure 3: General block diagram for CPC calibration using the soot aerosol generator.

There are several important features that go a significant way towards meeting the criteria for the procedure:

- An overflow is used that ensures that all parts of the experiment outside the fume cupboard are operating at a slight underpressure such that any leaks do not result in a release of nanoparticles. In practice, the differential pressure at the exit of the Differential Mobility Analyser (DMA) is <10 mbar below ambient atmospheric pressure, ensuring that the pumps in the detectors are working close to their normal conditions.
- The DMA selects particles with a narrow electrical mobility range. The size of these particles depends on the number of charges they carry, so the proportion of larger multiply charged particles depends on the raw aerosol size distribution. This has implications for the multiple charge correction discussed in the next section.
- The sampling lines used in the experiment are important. Although general guidance dictates that all sample lines should be as short and as straight as possible, and use suitable tubing material, the performance of the sample lines is only critical to the overall experimental performance after the DMA. At this point, the lines split to supply the reference and test instruments, so they must be as equivalent as possible and change the sample as little as possible. This includes the residence time of the lines, so a makeup flow may need to be used, which splits from the sample flow on one branch at the last possible moment.

The conventional calibration procedure is based on measuring particles in the 60-70 nm size range. The reason for choosing this size is that it offers the best practical compromise between ensuring that the CPC is measuring particles for which it has a nominal 100% detection efficiency, and avoiding excessive complications at larger particle sizes due to the increased probability of multiple charging. For this the CAST is generally set its D55 mode, which provides a broad particle size distribution peaking at around 55 nm.

The measurement schedule for the calibration is summarised in Figure 4.

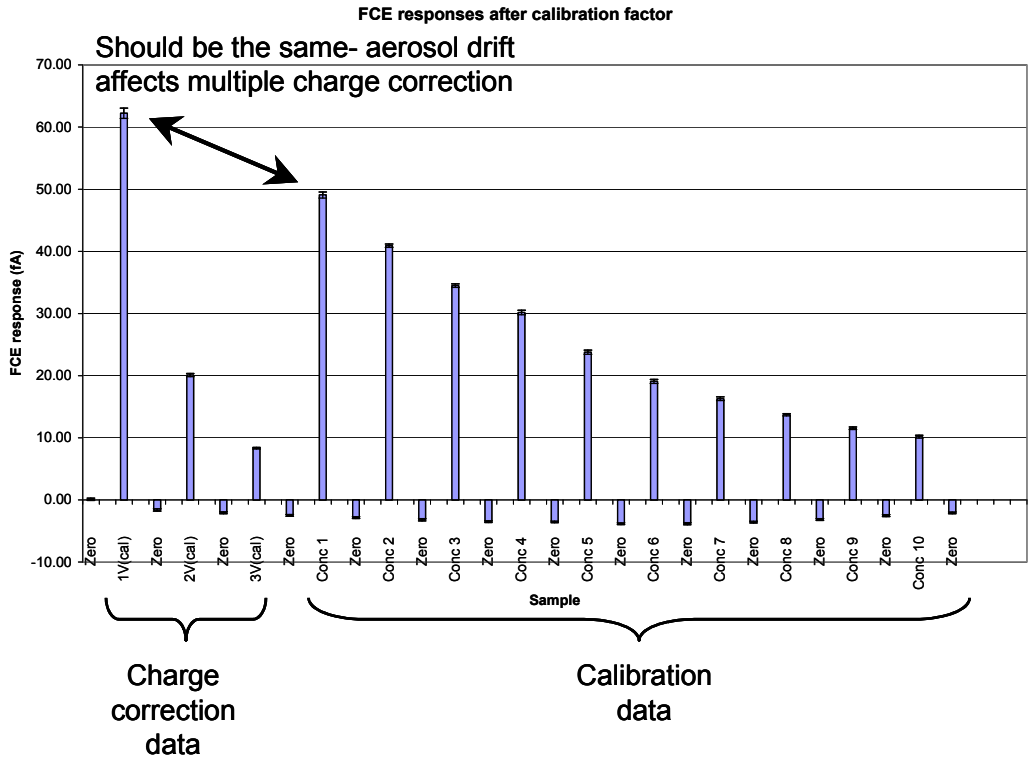

Figure 4: Example data collection schedule for the soot-based CPC calibration.

The following features should be noted:

- Between every data point, a zero is recorded. This is required because the zero-point of the aerosol electrometer drifts slightly. A linear interpolation is used to correct for this drift. The zero points are taken by setting the DMA voltage to zero.
- The multiple charge correction data consists of 4 data points, the last of which is also the first calibration data point. The first and last points are for identical settings at the desired particle size, so any variation in the concentration measured is due to drift in the particle generator. A linear interpolation drift correction is used to correct the middle two points, which are taken at double and triple the normally used DMA voltage.
- Each data point consists of a 5-minute sample (measured at 1 Hz and averaged) followed by a 2-minute equilibration period.
- The number concentration is varied through control of the CAST's built-in diluter.
- Throughout the experiment, the settings to be changed are always changed at the earliest possible moment:

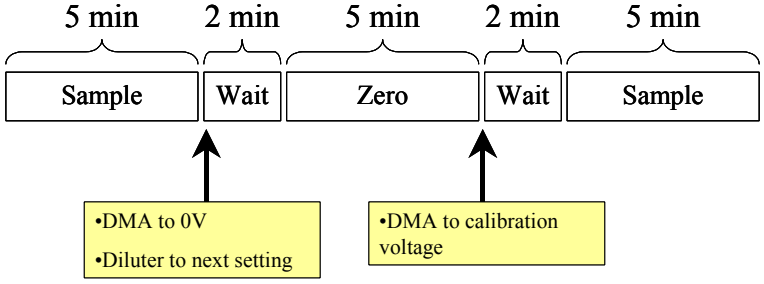

2.4.2 Data Analysis

The data analysis and uncertainty estimation are driven by the calibration record spreadsheet. There are slightly different versions of the spreadsheet for each variation in the calibration to allow for different numbers of data points to be collected, but the approach to data analysis is the same.

The equipment used for the calibration uses a DMA to provide the size and charge selectivity. The DMA passes a stream of particles with a narrow range in electrical mobility, which usually consists of a small proportion of larger multiply charged particles. The detectors therefore do not measure particles of a single size, but particles of a single electrical mobility. This means that the instrument response can be divided into components:

$$C_{\text{Meas,FCE}} = \sum_{i=1}^{n} iC_{d_i,q_i} \qquad (1)$$

$$C_{\text{Meas,CPC}} = \sum_{i=1}^{n} C_{d_i,q_i} \qquad (2)$$

where i represents the number of charges on the particle. This means that the two instruments respond differently if multiply charged particles are present. As such, a significant amount of effort is expended in removing this difference.

The experiment consists of two parts: the charge correction determination and the calibration itself. In the first part, the reference detector response is recorded (along with the test instrument responses for completeness and simplicity) for various multiples of the normal DMA operating voltage whilst keeping the particle generator settings constant. In the second part, the first calibration point is recorded for the same particle generator settings as the first part at the regular operating voltage to allow a correction to be applied for any drift in the output of the particle generator. Following this, the subsequent calibration points are recorded at the regular operating voltage but for different particle number concentrations. Every ‘voltage on’ data point throughout both parts is bounded by a ‘voltage off’ measurement. This provides a means to correct for any drift in the zero point of the reference instrument. The measurement timetable consists of 5 minutes measurement followed by 2 minutes adjustment and equilibration time.

The following discussion describes the data analysis and uncertainty estimation built into the calibration record spreadsheet. The case of a calibration requiring a 3-point multiple charge correction is used as an example. The treatment may easily be extended to further multiples of the normal operating voltage. The flow of the data analysis is summarised in the Figure 5.

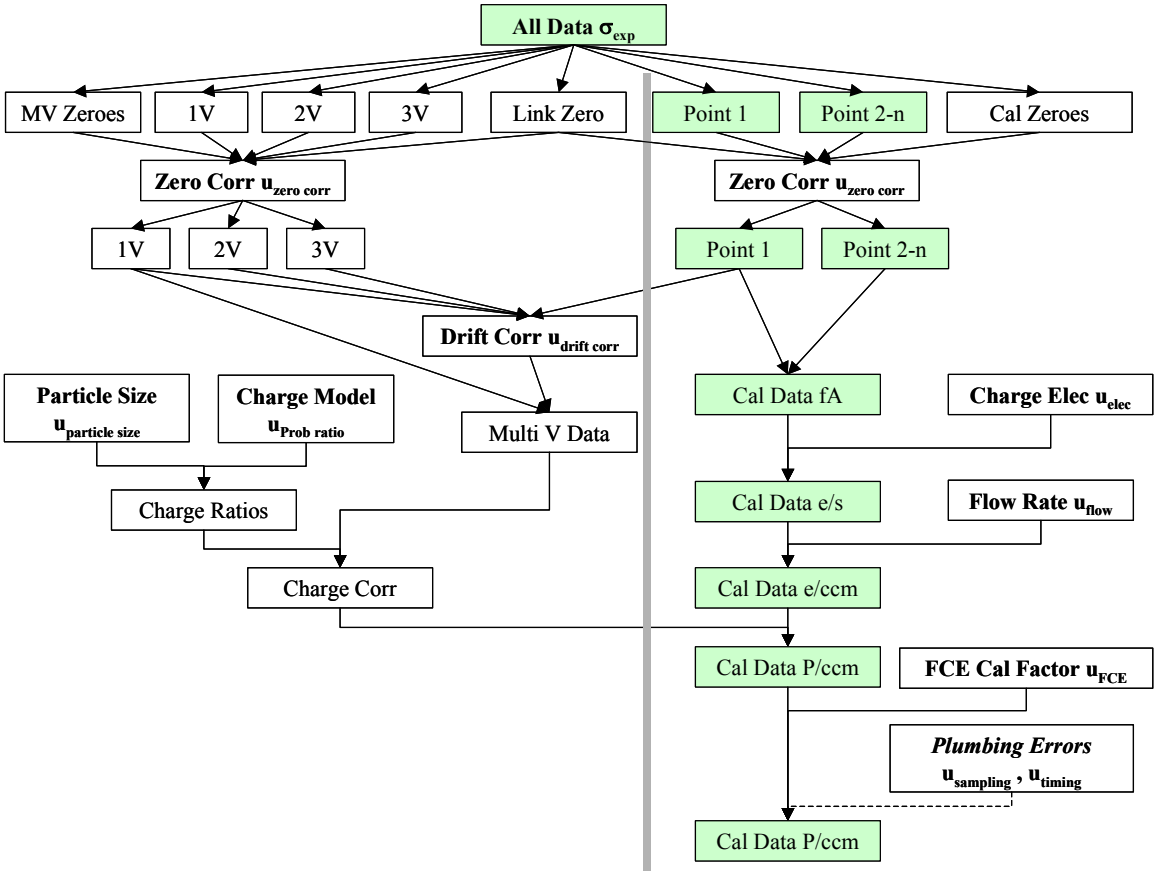

Figure 5: Flow diagram of CPC calibration data analysis.

The raw data, which consists of 1Hz time series is averaged into the 5-minute samples and the standard deviation calculated, σ_{Exp} for both the reference instrument and the CPC. This provides an estimation of the uncertainty due to random fluctuations in the experiment.

- The reference instrument data is recorded in units of fA.
- The CPC data is recorded in units of particles per cm^3. No further manipulation of the CPC data is undertaken.

A baseline correction is applied to the 'voltage on' reference instrument data using the adjacent zero points. It is assumed that drift in the baseline varies linearly over the timescales under consideration. The correction is calculated using:

$$I_{\text{corr}} = I_0 - \frac{Z_{pre} - Z_{post}}{2} \qquad (3)$$

The uncertainty in the magnitude of this correction is taken as:

$$u_{\text{Zero corr}} = \sqrt{{\sigma_{Z_{pre}}}^2 + {\sigma_{Z_{post}}}^2} \qquad (4)$$

The averaged, baseline corrected data points from the second part of the experiment (the calibration points) are then converted, in several stages, into a particle number

concentration taking into account the presence of multiply charged particles. The following conversions are carried out:

- Conversion from fA to es^{-1} (electrons per second) using the charge on the electron. The uncertainty contribution (although small) is given by u_{elec}.
- Conversion from es^{-1} to ecm^{-3} using the measured flow rate of the reference detector. This is measured using a mass flow meter and converted into a volumetric flow using the ideal gas equation. The uncertainty in the measured flow rate u_{Flow} is taken from the mass flow meter's calibration certificate.
- The calibration of the electrometer is applied. The zero offset is not required as this is normalised out by the zero correction procedure used above. The contribution to the standard uncertainty u_{FCE} is taken from the electrometer calibration certificate.
- The correction for the presence of multiply charged particles is calculated by determining the theoretical response ratio R_{Det} between the reference detector and the CPC. The uncertainty introduced by the application of this correction is given by $u_{\text{q corr}} = u_{R_{Det}} C_{\text{Meas}}$, where $u_{R_{Det}}$ is the relative uncertainty in R_{Det}. The determination of R_{Det} and $u_{R_{Det}}$ is discussed later. This yields the final particle number concentration.
- In addition, estimations of the uncertainty due to the sampling lines u_{Sampling} and timing mismatch between the instruments u_{Timing} are included. These are discussed in more detail below.
- The final contribution to the standard uncertainty is calculated by taking the square root of the sum of squares of each contribution. Typical values show that the claimed uncertainty can be met:

Source of uncertainty	Coverage factor	Value
Variation in reference detector reading	k=1	1.5%
Zero correction	k=1	0.1%
Charge on electron	k=1	0.1%
Reference detector flow rate	k=1	1.0%
Reference detector calibration	k=1	1.0%
Multiple charge correction	k=1	2.5%
Sampling	k=1	0.6%
Timing mismatch	k=1	0.2%
Combined standard uncertainty	k=1	3.3%
Expanded uncertainty	**k=2**	**6.6%**
All contributions have a normal distribution		

Figure 6: Example uncertainty budget for the soot-based CPC calibration.

The magnitude of the uncertainty due to the sampling lines u_{Sampling} consists of several contributions:

- Differential deposition in the sampling lines can lead to an error in the determined calibration factor. In an experiment using typical calibration conditions, but with an exaggerated difference in path length of a factor of 370%, the determined calibration factor was seen to change by 2.8%. Therefore, a 5% difference in path lengths would lead to an error of <0.1%.
- Any change in the charge distribution after the particles leave the DMA will affect the two instrument types differently. In a related experiment to the one described above, the sample lines to both the reference instrument and instrument under test were lengthened by 370%. The calibration factor was seen to change by 0.4%. Therefore, changing the length of the sample lines by a factor of 2 would lead to an error of <0.25%.
- Finally, the equivalence of the sampling lines was evaluated by swapping the lines for both a 2 and 4 instrument configurations. The largest deviation in the calibration factor observed was <0.5%.

Combining these contributions yields a combined sampling error of <0.6%, which is taken as a conservative estimate of the measurement uncertainty due to sampling.

An estimation of the uncertainty brought about by a worst-case 10 second timing mismatch u_{Timing} in the data collection was determined by calculating the average difference obtained in the reference instrument's average response when displacing the experimental data time series by 10 seconds.

Calculation of the multiple charge correction and its associated uncertainty is carried out in several stages. It makes use of the data from the first part of the experiment (multiples of the normal operating voltage) as well as the first point from the second part. Firstly, a correction is applied to take account of drift in the output from the particle generator:

$$I_{\text{2V, zero corr, drift corr}} = I_{\text{2V, zero corr}} - \frac{1\left(I_{\text{1V, zero corr}} - I_{\text{Conc1, zero corr}}\right)}{3} \tag{5}$$

$$I_{\text{3V, zero corr, drift corr}} = I_{\text{3V, zero corr}} - \frac{2\left(I_{\text{1V, zero corr}} - I_{\text{Conc1, zero corr}}\right)}{3} \tag{6}$$

The uncertainty due to this correction is assumed to be:

$$u_{\text{drift corr}} = \sqrt{\sigma_{\text{1V,exp}}{}^2 + u_{\text{1V,zero corr}}{}^2 + \sigma_{\text{Conc1,exp}}{}^2 + u_{\text{Conc1,zero corr}}{}^2} \tag{7}$$

This means that the overall uncertainty for the multiple voltage points $I_{\text{nV, zero corr, drift corr}}$ is given by:

$$u_{I_{\text{nV, zero corr, drift corr}}} = \sqrt{\sigma_{\text{nV,exp}}{}^2 + u_{\text{zero corr}}{}^2 + u_{\text{drift corr}}{}^2} \tag{8}$$

These corrected concentrations are then used to determine the theoretical response ratio[1] between the reference detector and a theoretical instrument under test using the instrument response equations for the reference instrument and the CPC. The i>1 terms of the reference detector response equation are calculated using the measured values of the multiple voltage points and knowledge of the particle size-dependent charging probabilities[2], discussed further in Section 3. The relative concentrations of particles of the same size and different charges can be calculated using

$$C_{d_n,q_n} = \frac{P_{d_n,q_n}}{P_{d_n,q_1}} C_{d_n,q_1} \qquad (9)$$

where d_n refers to particles with a size that corresponds to the electrical mobility due to a single charge at n times the normal operating voltage. Therefore, the nV data points can be used to estimate the i=n terms of the response equation at the normal operating voltage. The contributions to the instrument response get smaller as i increases. It is generally sufficient to terminate the Taylor series at i=3 or 4. For the latter case, it is necessary to carry out a second level of charge correction due to the 2V data itself being affected by doubly charged particles. This then allows the evaluation of the first term of the response equation:

$$C_{d_1,q_1} = C_{\mathrm{FCE,V}} - 2C_{d_2,q_2} - 3C_{d_3,q_3} \qquad (10)$$

The uncertainty in the i>1 terms is given by:

$$u_{C_{d_n,q_n}} = \sqrt{u_{\text{Prob ratio}}{}^2 + u_{C_{\text{Meas,nV}}}{}^2} \qquad (11)$$

The determination of $u_{\text{Prob ratio}}$ instead of the uncertainties associated with each probability is carried out because the dominant contributor to their uncertainties is correlated with the estimated particle size. Any systematic error in the size classification equipment will cause both particle sizes considered to err in the same direction (ie, bigger or smaller) and any random variation in the particle size being considered will be accounted for in the averaging of instrument response time series. Therefore, to quantify this systematic source of error, the relationship between the relative error in particle size and relative error in the probabilities ratio was determined. This means that the value of $u_{\text{Prob ratio}}$ is related to an estimated value of the systematic uncertainty in particle size, $u_{\text{Particle size}}$. A plot of this relationship for typical calibration conditions (Figure 7) yields suitable coefficients:

[1] As the ideal instrument under test concept is only used to calculate an expected response ratio, there is no need to convert the charge correction data points from current into number concentration, so we can say $C_{\text{Meas,nV}} \equiv I_{\text{3V, zero corr, drift corr}}$.

[2] J Aero Sci, Vol. 19, pp. 387-389 (1988)

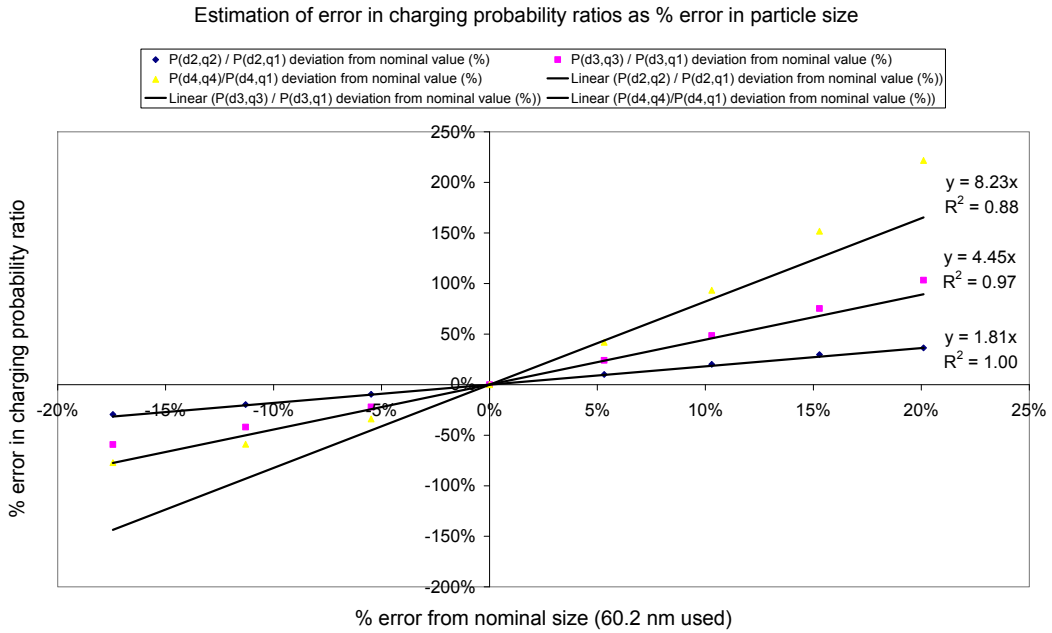

Figure 7: Estimation of the error in charging probability ratio due to error in the assumed particle size.

The uncertainty in the i=1 term is given by:

$$u_{C_{d_1,q1}} = \sqrt{\left(\frac{C_{\mathrm{FCE,V}}}{C_{\mathrm{FCE,V}} + 2C_{d_2,q_2} + 3C_{d_3,q_3}} u_{C_{\mathrm{FCE,V}}}\right)^2 + \left(\frac{2C_{d_2,q_2}}{C_{\mathrm{FCE,V}} + 2C_{d_2,q_2} + 3C_{d_3,q_3}} u_{C_{d_2,q2}}\right)^2 + \left(\frac{3C_{d_3,q_3}}{C_{\mathrm{FCE,V}} + 2C_{d_2,q_2} + 3C_{d_3,q_3}} u_{C_{C_{d_3,q3}}}\right)^2} \quad (12)$$

The theoretical test instrument response can then be calculated using:

$$C_{\mathrm{CPC_{Ideal},V}} = C_{d_1,q_1} + C_{d_2,q_2} + C_{d_3,q_3} \quad (13)$$

The uncertainty in this value is given by:

$$u_{C_{\mathrm{CPC_{Ideal},V}}} = \sqrt{\left(\frac{C_{d_1,q_1}}{C_{d_1,q_1} + C_{d_2,q_2} + C_{d_3,q_3}} u_{C_{d_1,q1}}\right)^2 + \left(\frac{C_{d_2,q_2}}{C_{d_1,q_1} + C_{d_2,q_2} + C_{d_3,q_3}} u_{C_{d_2,q2}}\right)^2 + \left(\frac{C_{d_3,q_3}}{C_{d_1,q_1} + C_{d_2,q_2} + C_{d_3,q_3}} u_{C_{C_{d_3,q3}}}\right)^2} \quad (14)$$

Finally, the ratio of the measured reference detector response and theoretical CPC response is calculated to yield R_{Det}. The uncertainty in this ratio is given by:

$$u_{R_{Det}} = \sqrt{u_{C_{\mathrm{CPC_{Ideal},V}}}^{\ 2} + u_{C_{\mathrm{Meas,V}}}^{\ 2}} \quad (15)$$

2.4.3 Results

Repeated tests of this procedure have shown that it is consistent and the results are very close to those expected. Most work has been done using soot particles, but some initial results for atomized NaCl are presented also.

Figure 8 shows the calibration factors determined for all tests carried out along with their associated uncertainties. The test calibrations were carried out over the period of approximately 1 month using the same test CPC. All except one dataset used 5 points for the calibration as this was found to be suitable for testing purposes. The remaining dataset consisted of 10 points, but was not found to offer enough additional benefit to warrant the extra time expenditure in the testing phase.

The calibration factors obtained for soot particles in the photometric mode concentration range (nominally 10 000 cm^{-3} to 100 000 cm^{-3}) are very consistent and implies that the CPC used is precise but inaccurate in photometric mode. The small size dependence of the calibration factors obtained is an important sign that the multiple charge correction is functioning as hoped. Furthermore, the calibration carried out in single particle mode (ie at low concentration) has a calibration factor very close to unity, providing extra confidence in the charge correction methodology.

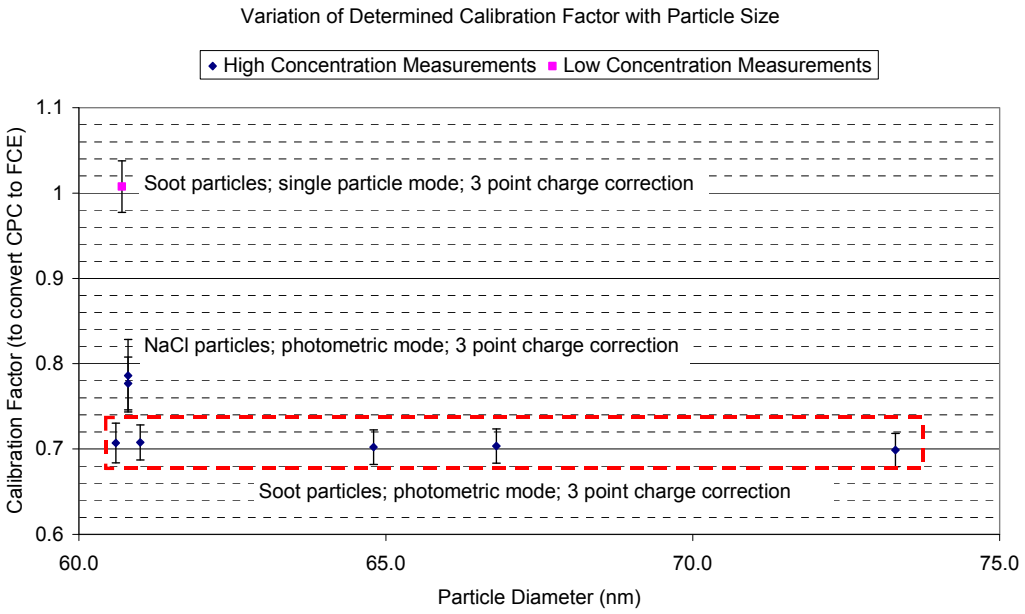

Figure 8: Summary of test calibration results using the NPL CPC calibration procedure. Error bars are standard (k=1) uncertainties.

The two NaCl calibrations do not align closely with the soot data, though they agree at the 95% confidence ($k = 2$) level. There are two likely reasons for this:

1. The raw aerosol size distribution is broader than that for soot, meaning that the DMA will allow through a relatively greater number of larger, multiply-charged particles, and a 4-point multiple charge correction is probably required.
2. The practicalities of keeping the aerosol stable and within the required concentration range were still being refined, so the confidence in the data is much lower.

The fact that the expanded (k = 2) uncertainties for all of the photometric calibrations overlap implies that there are no critical material-dependent effects being observed. Future data collection will help improve confidence in the results, particularly for NaCl.

The magnitude of the multiple charge correction factors used in these test calibrations is presented in Figure 9.

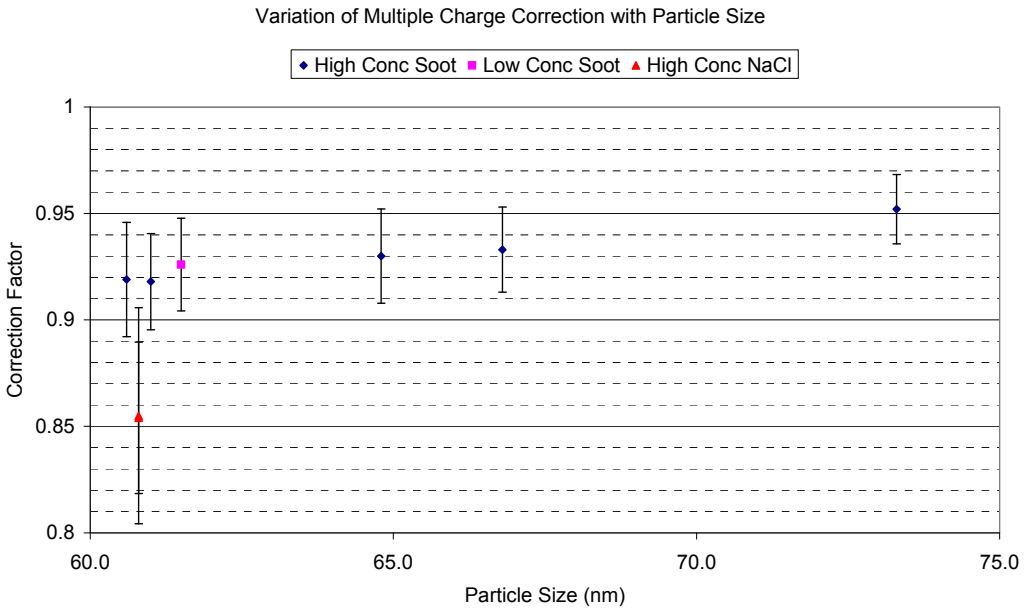

Figure 9: Values for the multiple charge correction used in the NPL CPC calibration.

The magnitude of the correction is seen to vary steadily with particle size for the soot-based calibrations. The deviation from unity is seen to decrease as with increasing particle size. This is to be expected because, despite the presence of more multiply charged particles at larger sizes, the drop-off in the raw aerosol size distribution more than compensates for this. The corrections for the NaCl calibrations show a higher deviation from unity than the soot. This is in line with expectations due to the broader raw aerosol size distribution. The larger error bars in comparison to the soot data points are a reflection of the experimental difficulties encountered.

Overall, these results indicate that a robust and transferable CPC calibration procedure has been developed, although there is some work still to do in transferring the procedure from the soot case study to other materials. The work presented here has also been used as supporting evidence for the UKAS accreditation of this procedure.

3 Particle Charging Effects

A central component of the CPC calibration procedure is the correction for the presence of multiply charged particles. This correction, and the data processing algorithms for many other airborne nanoparticle instruments, relies heavily on the size-dependent particle charging probability distribution (usually simply referred to as the charge distribution). As such, it is important to have confidence in this distribution and its operational feasibility.

The almost universally accepted bipolar charge distribution in use is based on an approximation of Fuchs' charge distribution carried out by Wiedensholer[3] some 20 years ago. Two relationships were used for differing number of elementary charges. For single or doubly charged particles, a fit to a corrected version of Fuchs theory was used to determine the charging probabilities for positive and negative polarities (a difference in the mobility of the positive and negative air ions leads to this difference). This is only applied above 20 nm for doubly charged particles. For greater numbers of charges, the relationship determined by Gunn in 1956 was used above 70 nm. This does not distinguish between polarities. Wiedensholer provides no justification for this switch in model. This means that there is certainly some work to be done in evaluating the uncertainties surrounding these approximations.

There is much experimental evidence showing that Wiedensholer's approximation is based on sound theory, which has no doubt aided its adoption. However, this assumes that the charge neutralisation methods used have sufficient capacity to reach the required steady state. Furthermore, most neutralisers use a radioactive source that severely reduces the transportability of the instruments for administrative reasons. Therefore, the usefulness of alternative neutralisation methods should be considered.

There are very few commercially available, non-radioactive charge neutralisation devices suitable for use with instruments such as the Scanning Mobility Particle Sizer (SMPS). The unit obtained by NPL for this work features the ability to introduce an excess of positive and/or negative ions, generated by corona discharge, into the sample in varying amounts using a particle free sheath air flow, causing a dilution of the sample in the process. At best, it was found that the neutraliser caused at least a factor of 10 dilution of the sample number concentration.

The effect of applying both positive and negative unipolar as well a bipolar ion concentration is illustrated in Figure 10. Several different size distributions, measured by the same SMPS, can be observed:

- The distributions obtained using either of the bipolar neutralisation methods are effectively indistinguishable, implying that bipolar electrical neutralisation is a satisfactory alternative to the traditional radioactive method.
- The distributions obtained for the two unipolar cases demonstrate the effectiveness of the charging process. For the negatively-charged case, negligible signal is observed, which is to be expected because the SMPS (in this case) detects only positively charged particles. Conversely, the positive case

[3] J Aero Sci, Vol. 19, pp. 387-389 (1988)

shows enhanced signal, with the peak maximum being shifted to a smaller size due to high levels of multiple charging.

- Comparison of the size distribution for un-neutralised particles to the neutralised cases illustrates the necessity of the neutralisation process.

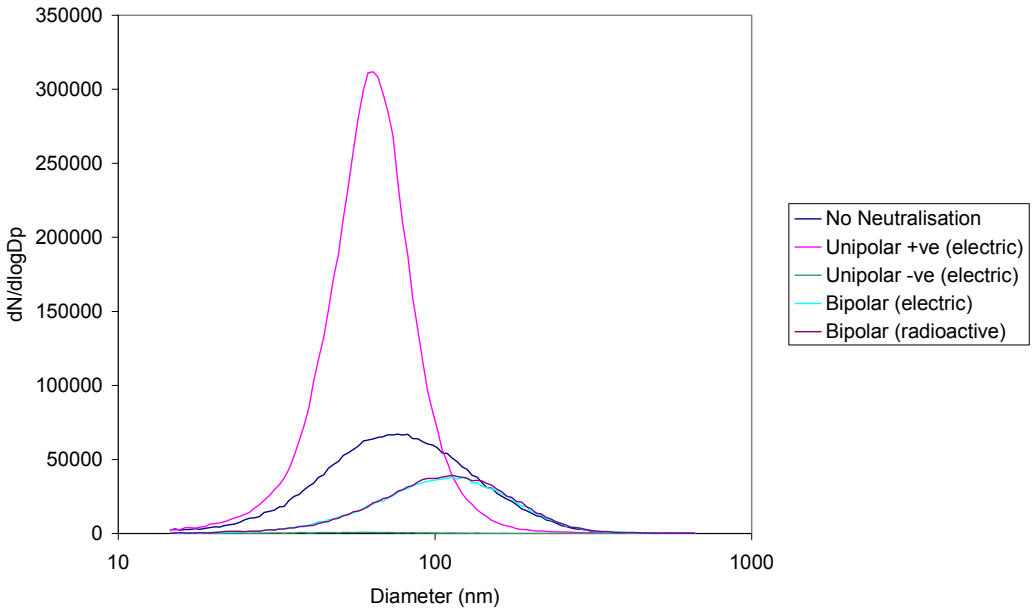

Figure 10: Effect of neutralisation method on the measured SMPS size distribution.

The electrical neutraliser was then used to test the ability of the standard radioactive neutraliser to rectify the charge distributions of samples that themselves have extreme charge distributions by placing the two neutralisers in series and challenging the SMPS and SMPS+E (a DMA with an electrometer rather than a CPC detector), with a 26 nm soot aerosol.

Figure 11 shows the effect of this pre-neutralisation on the peak profile of the air ions that can be detected using the SMPS+E instrument. These ions are those usually responsible for the charging of larger particles, and any changes observed indicate a change in the concentration of ions present, and therefore a possible deviation in the charge distribution adopted by any particles present. Figures 12 and 13 show the small effect of the pre-neutralisation process on the measured data. However, these changes are of a similar magnitude to the scan-to-scan variation in the data, and given the extremity of the rather contrived test conditions it appears that the neutraliser is capable of dealing with extreme incident charge distributions.

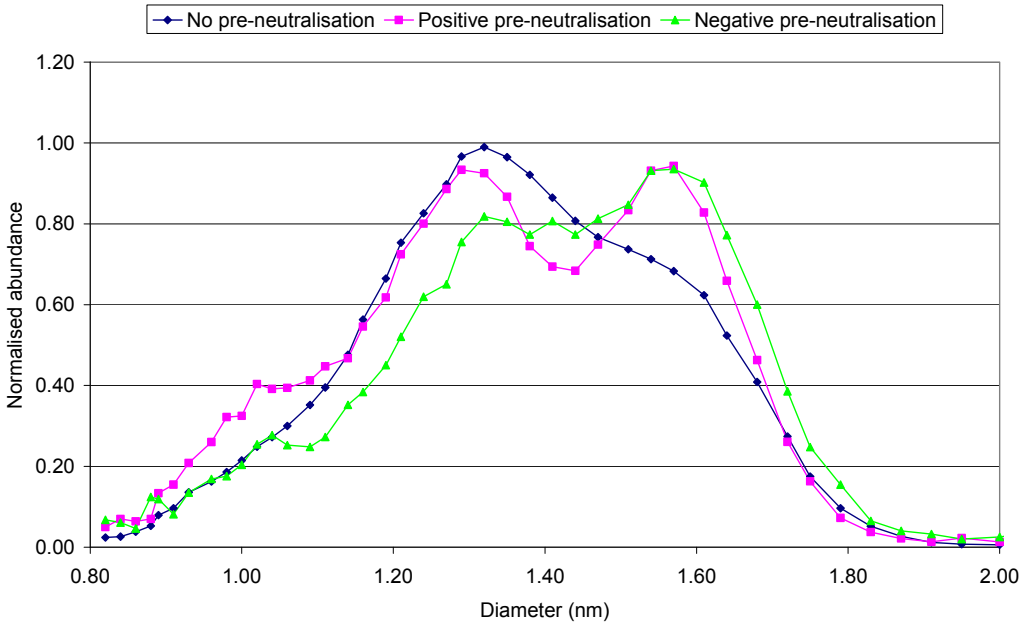

Figure 11: Effect of pre-neutralisation on the air ion peak measured by the SMPS+E.

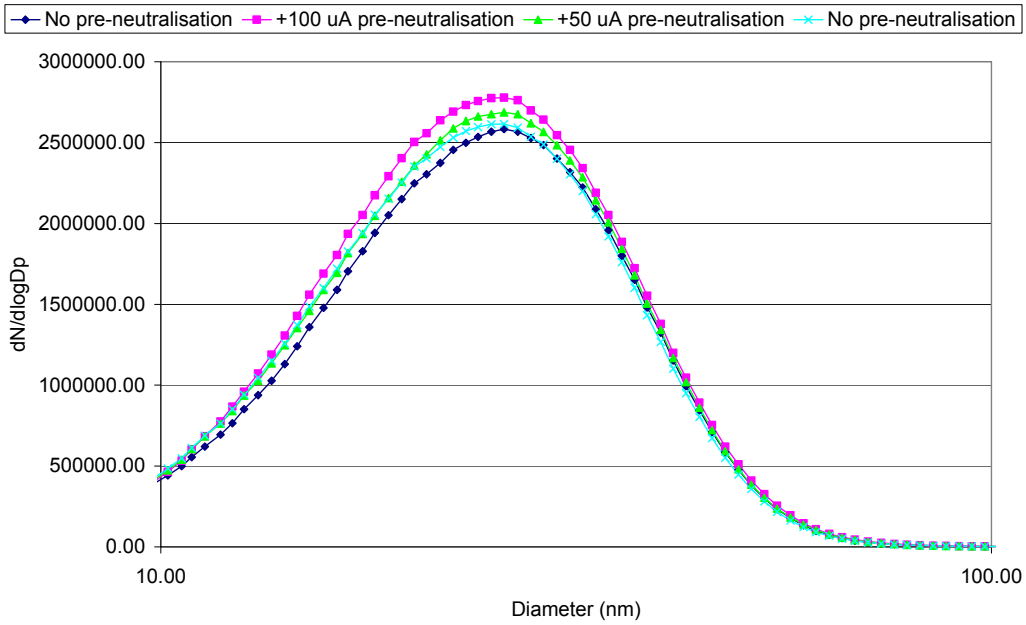

Figure 12: Variation in the measured size distribution due to positive pre-neutralisation. Data was recorded using a TSI3 936L22 SMPS fitted with the 3085 nDMA.

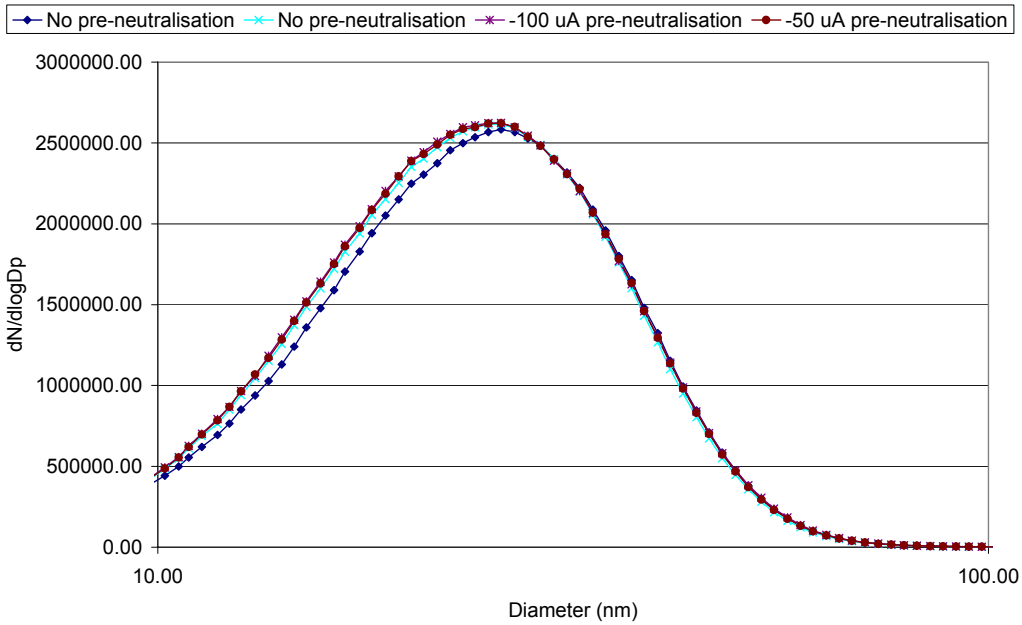

Figure 13: Variation in the measured size distribution due to negative pre-neutralisation. Data was recorded using a TSI3 936L22 SMPS fitted with the 3085 nDMA.

The 26 nm aerosol used in the above experiments is also suitable for testing both SMPS instruments at the extremes of their size ranges. The SMPS+E fitted with the short DMA is limited in its size range by the desirability to measure in the 1 nm size range at one extreme and by the need to prevent arcing in the DMA at high voltages. In contrast, the detection threshold of the CPC detector is the main limiting factor for the conventional SMPS. However, these measurement ranges overlap, meaning that they may be compared. The comparison of the SMPS+E and the conventional SMPS fitted with the short DMA is shown in Figure 14. The output of the SMPS software with and without the charge and diffusion correction algorithms enabled is also included. The size prediction of the two instruments is comparable, but the concentrations predicted are significantly different.

Similar results for the long DMA are illustrated in Figure 15. Again, the size-related information is approximately correct, but the concentration information is rather disappointing. Also, the severe action of the diffusion correction algorithm is very evident, highlighting significant data interpretation issues.

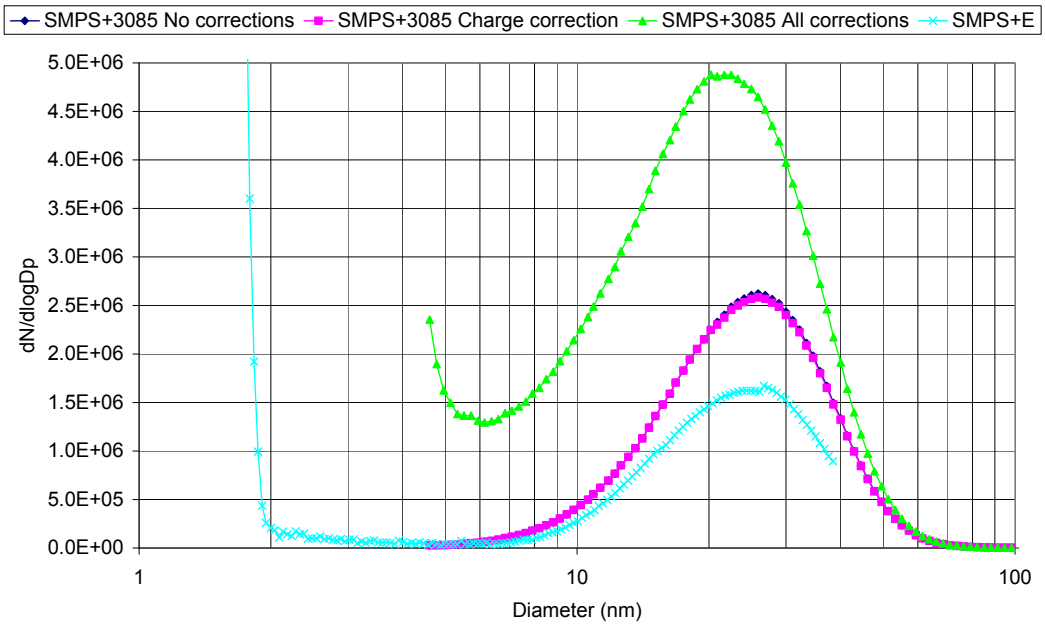

Figure 14: Comparison of the SMPS+E and TSI3936L22 SMPS fitted with the 3085 short DMA.

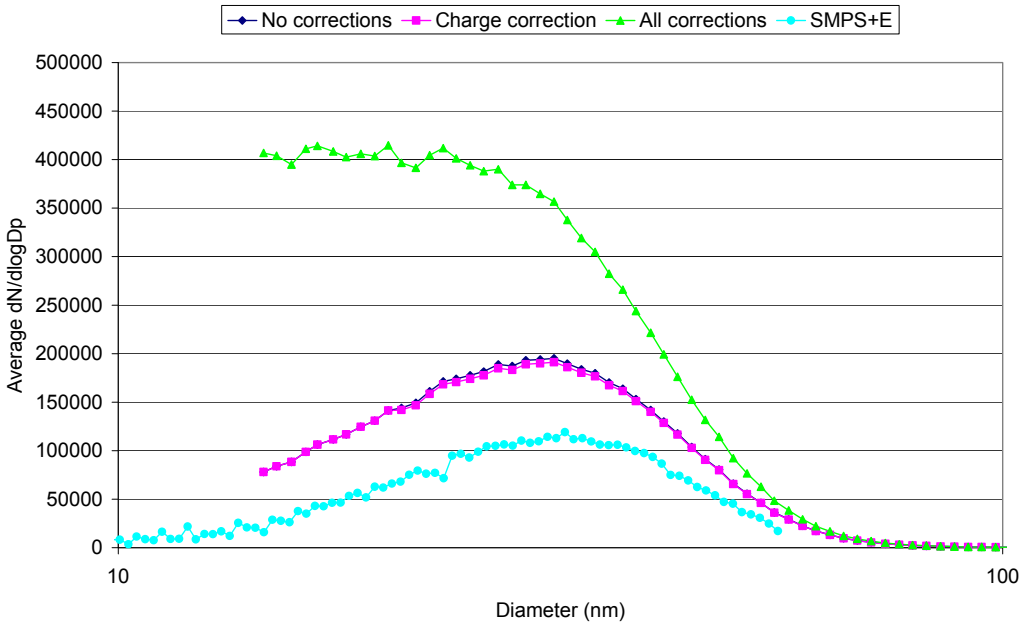

Figure 15: Comparison of the SMPS+E and TSI3936L22 SMPS fitted with the 3085 long DMA.

4 DMA simulation

An important quality assurance aspect of the CPC calibration procedure is determining the actual size(s) of particles being measured. This is primarily governed by the performance of the Differential Mobility Analyser (DMA).

The DMA is used to separate particles according to their electrical mobility. This is a property that is related to the particle aerodynamic diameter. For a given set of parameters, particles with a narrow range of electrical mobilities will pass from the inlet of the DMA to the outlet, where in practice they are often transported to a particle number counter. It consists of an annular space defined by two electrodes- the outer wall and the central rod. The outer wall is usually earthed and a high voltage supply connected to the inner rod. The sample to be classified is introduced as a thin flow to the outside of the annular space and an amount of clean sheath air to the remainder, both under well defined flow conditions. The sample exit slot is a small opening at the lower end of the inner rod, whose flow rate is well defined. Any air not exiting through the outlet slot leaves through the bottom of the DMA. This assembly is shown in Figure 16.

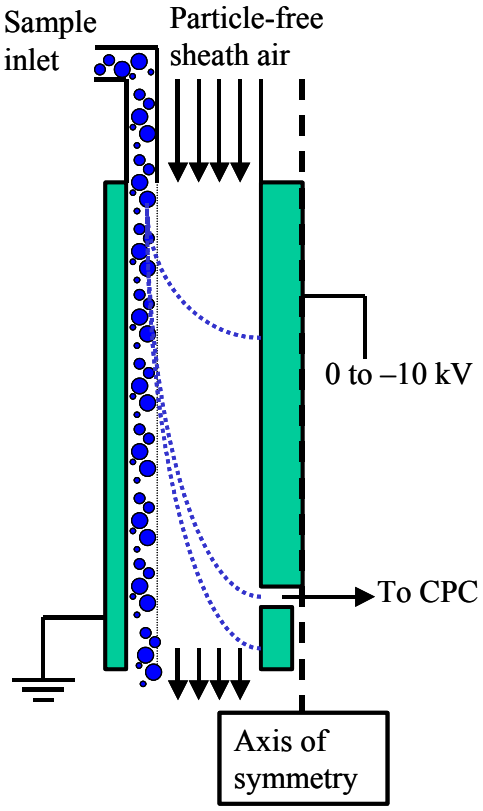

Figure 16: Schematic of the DMA.

Many parameters associated with the DMA affect the size of particles that pass to the exit slot. Parameters that may be varied include:

- Flow rates
- DMA geometry
- Rod voltage
- Empirical parameters describing particle behaviour.

Due to the finite widths of the inlet and outlet, the DMA passes a distribution of electrical mobilities to the exit slot, which is important when interpreting experimental data. This distribution is known as the transfer function. As such, it is desirable to use an appropriate model of DMA behaviour for experimental analysis.

There are three common means that this behaviour is determined:

1. By experiment
2. By theory, using analytical calculations.
3. By theory, using numerical calculations.

All three of these approaches have been used in the past, but the most promising seems to be the latter. As such, software was written to simulate the performance of the DMA.

The model used was based on calculating the progress of particles through the DMA over a large number of finely spaced time points for a range of different particle sizes. Through analysis of the trajectories the particles follow, the transfer function and other information can be determined. As the final results depend on statistical analysis, the trajectories of a large number of particles must be calculated. This algorithm is Monte-Carlo-like in style, although it does not feature a random number-driven component.

The DMA is to be modelled as a 2-Dimensional system. Radial and axial coordinates, *r* and *z*, define the position of the particle. Positive *z* is in the stream-wise direction. The position of the particle is calculated over a series of small time steps. The displacement of the particle on each time step is calculated from the radial and axial components of the particle velocity, which for the case of a non-diffusing particle are:

$$dr = \left[u_r(r,z) + Z_p E_r(r,z)\right]dt \qquad (16)$$

$$dz = \left[u_z(r,z) + Z_p E_z(r,z)\right]dt \qquad (17)$$

where:

- $u_r(r,z)$ is the radial component of the flow field within the DMA.
- $u_z(r,z)$ is the axial component of the flow field within the DMA.
- Z_P is the electrical mobility of the particle.
- $E_r(r,z)$ is the radial component of the electric field within the DMA.
- $E_z(r,z)$ is the axial component of the electric field within the DMA.

In this first version of the program diffusion was neglected, but it can be added at a later date if the need arises. All particles are assumed to be spherical.

The flow field and electrical field within the DMA are a function of the DMA geometry. The electrical mobility is a function of the particle and carrier gas properties.

Figure 17 illustrates the simplified model of the DMA geometry used.

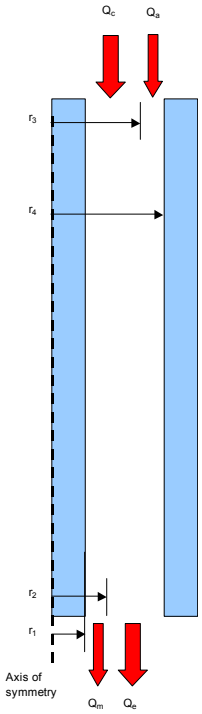

Figure 17: Schematic of the simplified DMA geometry.

This allows a number of simplifications to be made, meaning that the basic model is defined by the following parameters:

- r_1 is the inner rod radius.
- r_2 is the radius of the exit.
- r_3 is the radius of the aerosol inlet.
- r_4 is the outer wall radius.
- L is the length of the DMA classification region.
- Q_C is the clean sheath air flow rate.
- Q_A is the aerosol inlet flow rate.
- Q_E is the exhaust aerosol flow rate.
- Q_M is the monodisperse sample flow rate.

In this simulation, the sheath air loop is closed, as this is the normal mode of operation for modern DMAs, meaning that:

$$Q_E = Q_C \qquad (18)$$

$$Q_A = Q_M \qquad (19)$$

After this, the values of r_2 and r_3 can be calculated based on the flow field model used. The positions of these should be placed such that the correct fraction of gas flux, as defined by the various flow rates, passes each side of the inlet and outlet radii.

The two flow models implemented in this version are for plug and parabolic flow. Knowledge of the gas velocity at each point in space inside the DMA is essential both for setting up and running the simulation.

- Plug flow assumes that the axial velocity of the gas inside the DMA does not vary as a function of distance from the walls. Therefore, the velocity is simply the total DMA flow rate divided by the cross-sectional area of the DMA cavity.
- Parabolic flow assumes that gas flows more slowly near the walls. It can be described using the relationship[4]:

$$u(r) = 2u_{av}\frac{1-\left(\frac{r}{r_4}\right)^2+\left(\frac{k^2-1}{\ln k}\right)\ln\left(\frac{r}{r_4}\right)}{\frac{1-k^4}{1-k^2}-\frac{k^2-1}{\ln k}} \qquad (20)$$

where

$$k = \frac{r_1}{r_4} \qquad (21)$$

$$u_{av} = \frac{Q_a + Q_c}{\pi\left(r_4^{\,2} - k^2 r_4^{\,2}\right)} \qquad (22)$$

Equation 22 is equivalent to the velocity calculated using the plug flow model.

The flow rate found inside a certain radius in the DMA can be found by evaluating the following integral:

$$F(r_u) = \int_{r_1}^{r_u} u(r)dr \qquad (23)$$

Evaluation of this integral is used to determine the radial coordinates of the inlet, outlet and the initial positions of the particles at the start of the simulation.

After the DMA geometry has been defined, the initial (t = 0) positions and velocities of the particles must be described:

- The axial coordinate of all particles is set to zero. This is the point where they enter the classifier and experience the electric and flow fields that govern their trajectories.

[4] J. Chem. Eng. Japan **19**, 401-407.

- The radial coordinate of each particle should be set between r_3 and r_4, with an appropriate weighting for the flow rate such that there is a uniform number density of particles.
- The axial velocity should be calculated using the appropriate relationship described above for the chosen flow model.
- The radial velocity is the product of the electric field and electrical mobility of the particle. The electrical mobility is calculated using:

$$Z_p = \frac{q_p e C(d_p)}{3\pi\eta d_p} \qquad (24)$$

where

- q_p is the charge on the particle. This should be set to unity and will usually be the opposite polarity to the inner electrode voltage.
- e is the charge on an electron.
- $C(d_p)$ is the Cunningham slip correction.
- η is the gaseous viscosity.
- d_p is the particle diameter.

The Cunningham slip correction helps deal with the transition from microscopic to macroscopic theory. It takes the following form:

$$C(d_p) = 1 + \left(\frac{2\lambda}{d_p}\right)\left(A + Qe^{-\beta\left(\frac{d_p}{2\lambda}\right)}\right) \qquad (25)$$

where

- λ is the mean free path of the carrier gas.
- A, Q and β are experimentally determined constants.

The electric field is calculated using:

$$E_r = \frac{V}{r \cdot \ln\left(\frac{r_1}{r_4}\right)} \qquad (26)$$

When outside of the classifying region, the electric field is zero. There is no axial component to the electric field.

Following the calculation of the positions and velocities of each particle at t = 0, the algorithm then steps through time, using the velocities calculated in the previous iteration to calculate the new positions via equations 16 and 17. The velocities of the particles are then recalculated in the same way as for t = 0, with the following conditions applied:

- If the particle touches the wall of the DMA, the particle sticks and is deemed to have completed it trajectory.
- If the particle passes outside the region of the electric field, then it has completed its trajectory.

Clearly, once all particles meet these criteria, then the trajectory simulation is complete.

4.1 Validity of simulation

The results obtained using this algorithm compare well to experimental values. Figure 18 compares the experimental and calculated centroid mobilities determined over a range of parameter sets and DMA models.

DMA Model	Rod Voltage (V)	Sheath Air Flow Rate (lpm)	Sample Air Flow Rate (lpm)	Calculated Diameter (nm)	Experimental Diameter (nm)	% error	Comment
3081	-1000	3.0	0.3	152.2	153.3	-0.7%	--
3081	-1000	15.0	1.5	60.4	61.4	-1.6%	Experimental sample flow rate not exactly 1.5 lpm
3081	-5000	3.0	0.3	469.1	469.2	0.0%	--
3081	-1000	3.0	0.6	152.5	--	--	Not possible to test experimentally
3085	-1000	3.0	0.3	45.0	46.0	-2.2%	--
3085	-1000	15.0	1.5	19.5	20.1	-3.0%	Experimental sample flow rate not exactly 1.5 lpm
3085	-5000	3.0	0.3	110.2	111.3	-1.0%	--
3085	-1000	3.0	0.6	45.3	--	--	Not possible to test experimentally
Grimm Nano	1000	15.0	1.5	13.7	13.7	0.0%	--
Grimm Nano	1000	20.0	2.0	11.8	11.8	0.0%	--
Grimm Nano	5000	15.0	1.5	31.2	31.4	-0.6%	--
Grimm Nano	1000	15.0	3.0	13.7	13.7	0.0%	--

Figure 18: Summary of the comparison between the calculated and experimental transfer function maxima.

4.2 Effect of uncertainty in key parameters

The effect of uncertainty in the main parameters was investigated to determine their likely effect on the transfer function. To do this, the parameters describing a DMA operating under a set of standard conditions were systematically varied. The system used was a simplified model of the TSI 3081 DMA, running at a rod voltage of 1000 V, and with sheath and sample flow rates of 3.0 and 0.3 lpm respectively. This is representative of this DMA working as part of an SMPS system.

4.2.1 Cunningham Slip Correction

The Cunningham slip correction is an empirically determined set of parameters that modifies the mobility of particles when their size is comparable to the mean free path of the gas through which it is travelling. It can be thought of as a means to resolve the discontinuity between the microscopic and macroscopic models of particle motion. Several set of parameters have been determined over the last century and the effect of

implementing each should be examined to determine if serious systematic errors might be introduced by their inconsistent use. The sets implemented in DMAs are summarised in Figure 19.

Input string	Mean Free Path (m)	Correction term alpha	Correction term beta	Correction term gamma	Viscosity (kg m-1 s-1)
KIM_05_TAB1_1911	6.73E-08	1.034	0.536	1.219	1.82E-05
KIM_05_TAB1_1923	6.73E-08	1.209	0.406	0.893	1.82E-05
KIM_05_TAB1_1982	6.73E-08	1.155	0.471	0.596	1.83E-05
KIM_05_TAB1_1985	6.73E-08	1.142	0.558	0.999	1.83E-05
KIM_05_TAB1_1990	6.73E-08	1.209	0.441	0.779	1.83E-05
KIM_05_TAB1_1995	6.73E-08	1.231	0.496	1.178	1.83E-05
KIM_05_EXP	6.73E-08	1.165	0.483	0.997	1.83E-05
HUTCHINS_1995	6.73E-08	1.231	0.4695	1.1783	1.83E-05
ALLEN_1985_67p3	6.73E-08	1.142	0.558	0.999	1.83E-05
ALLEN_1985_65p3	6.53E-08	1.177	0.575	0.969	1.83E-05
KIM_2005_TEST	6.73E-08	1.165	0.483	0.997	1.83E-05

Figure 19: Summary of the slip correction parameter sets. Input strings refer to the references given in the user specification

The input strings refer to different sets of parameters that have been published. These represent the majority of parameterisations that have been published to date[5].

The standard operating conditions were used to calculate the transfer function for the DMA using each parameter set, except KIM_2005_TEST, which is used for program testing purposes only. The calculated transfer functions for each slip correction set are shown in Figure 20.

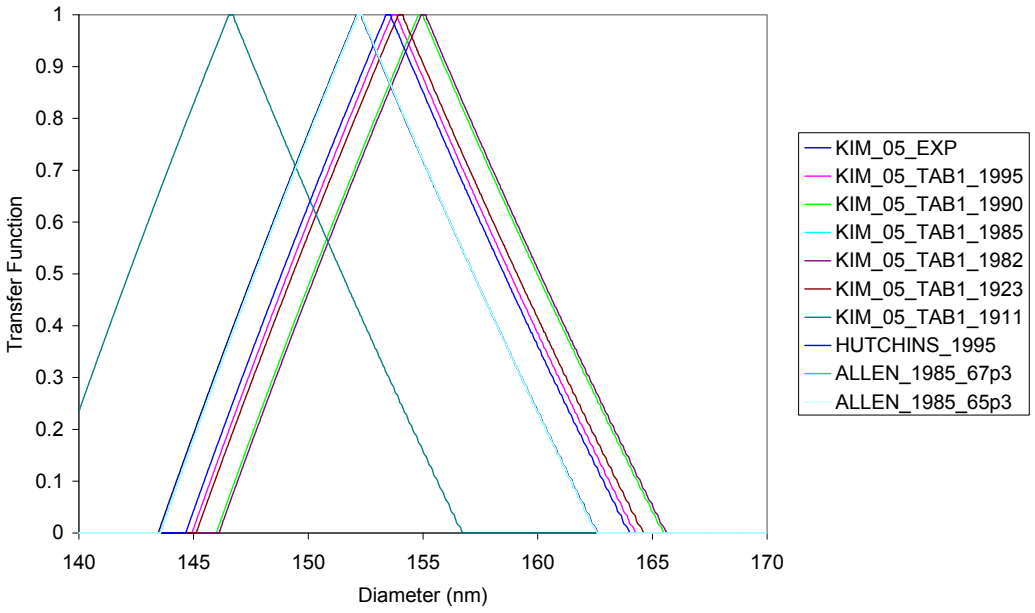

Figure 20: Comparison of the transfer functions obtained for each slip correction parameter set for the 3081 DMA (operating at 1000V with a 3.0/0.3 lpm flow rate configuration).

Figure 20 shows the variation in centroid mobilities for each parameter set, while Figures 21 and 22 compare their mean values. From these plots, it can be seen than a systematic error of the order of 1% can be expected if parameter sets are used inconsistently (assuming that the '1911' set is ignored). This compares well to the

[5] J. Res. Nat. Inst. Stand. Technol. **110** (1) 31-54, Aerosol Sci. Technol. **4**, 269-286 and Aerosol Sci. Technol. **22**, 202-218

operational resolution of the instrument. For a logarithmically spaced set of size bins with 64 bins per decade (in practice this is limited by vendor-supplied software), the relative size step at ~150 nm is approximately 3.7%. This means that the slip correction is effectively known to a greater degree of precision than the resolution of the instrument *at this particle size*. The means for further investigation are now in place, facilitating subsequent work as required.

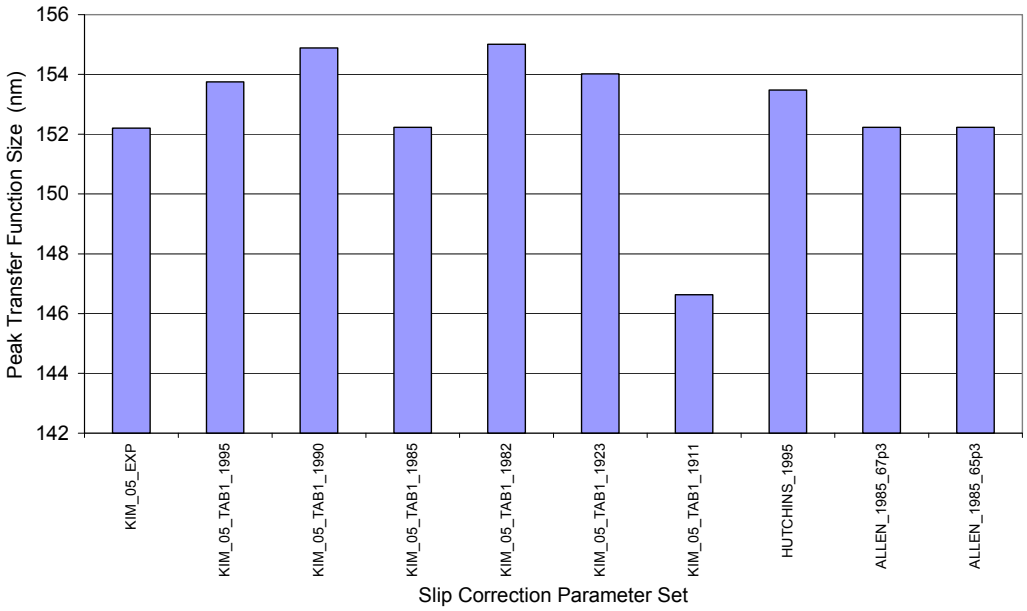

Figure 21: Centroid mobilities obtained with each slip correction parameter set using the typical DMA parameters.

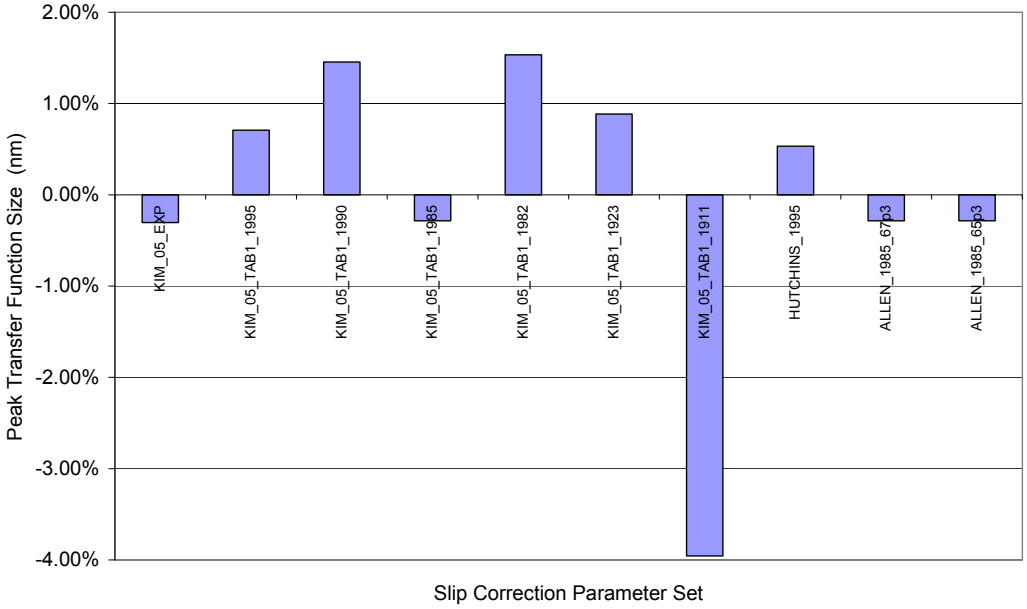

Figure 22: Variation in the centroid mobility due to slip correction parameter set expressed as a relative deviation from the mean.

4.2.2 DMA rod voltage

A more easily appreciated parameter that affects the DMA transfer function is the magnitude of the electric field used. To quantify this error, the variation in the centroid mobility as a result of a variation in the rod voltage from the ideal value was calculated. The result is shown in Figure 23. The variation observed is again smaller than the operational precision of the DMA as long as the HV source is accurate to better than 5%.

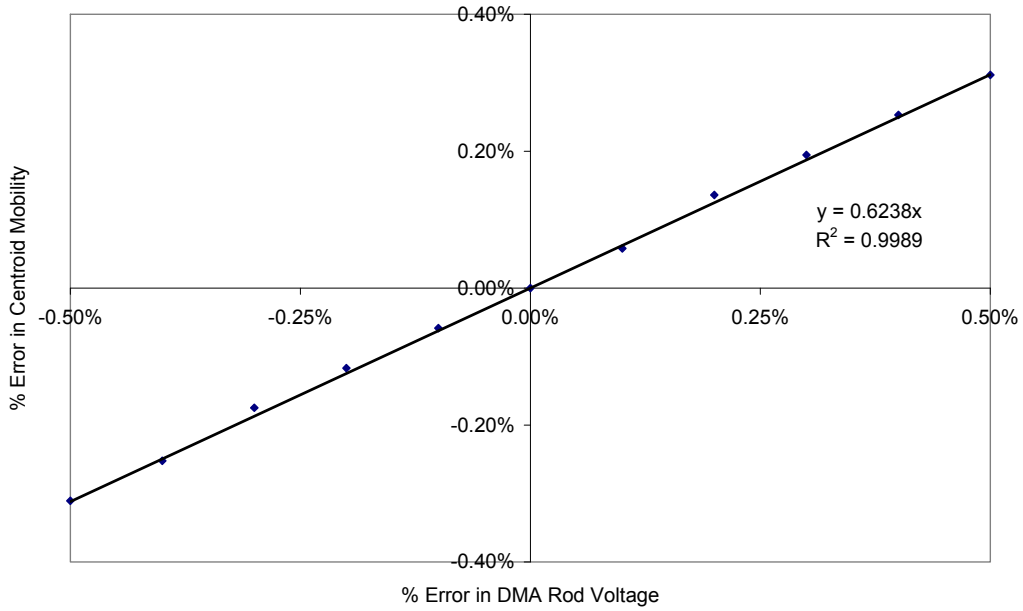

Figure 23: The relative uncertainty in centroid mobility due to deviation of the rod voltage from normal operating conditions.

4.2.3 Sheath air flow rate

This parameter has several effects on the transfer function. These include the centroid mobility, transfer function width and the residence time within the DMA, although this is only relevant when making a time-dependent measurement such as is done with the SMPS. The relative variation in centroid mobility when varying this parameter is illustrated in Figure 24. A relationship of similar magnitude is observed as was seen with the variation in rod voltage. The flow rate in the SMPS is measured using a mass flow meter, meaning that variation in flow rate of <5% can be expected. This means that the expected error due to variation in this parameter is less than the resolution of the SMPS.

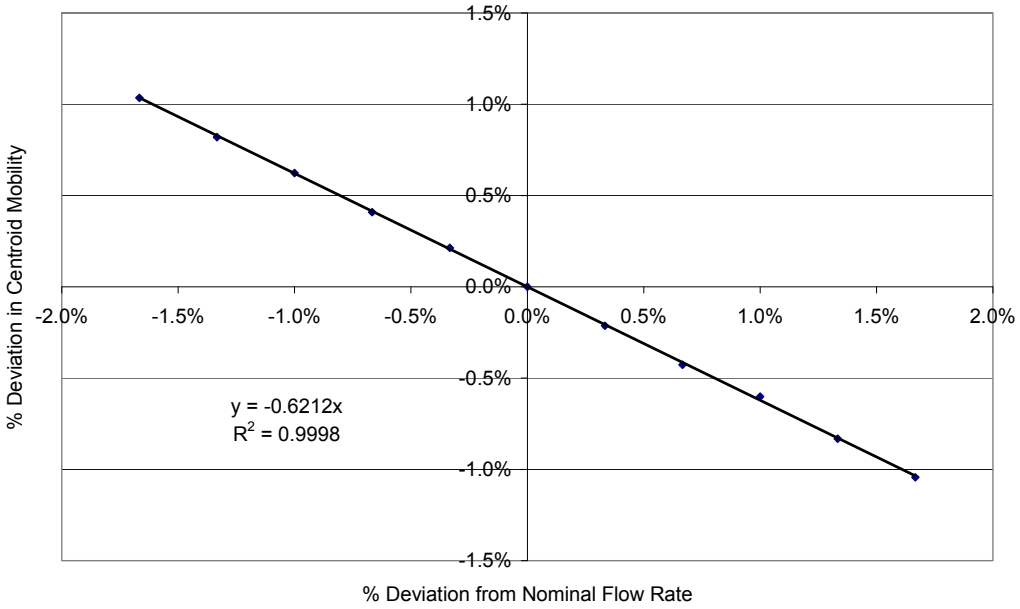

Figure 24: The relative uncertainty in centroid mobility due to deviation of the sheath air flow rate from normal operating conditions.

4.2.4 Sample air flow rate

The sample air flow rate primarily has an effect on the width of the transfer function. Deliberate variation of the ratio between the sheath and sample flow rates is a useful method for tuning the performance of a DMA being used for CPC calibration. Figure 25 shows the variation in transfer function due to this. The centroid mobility does not change by a measurable amount and the change in transfer function width will only have an effect on the size distribution reported for the extremely monodisperse aerosols.

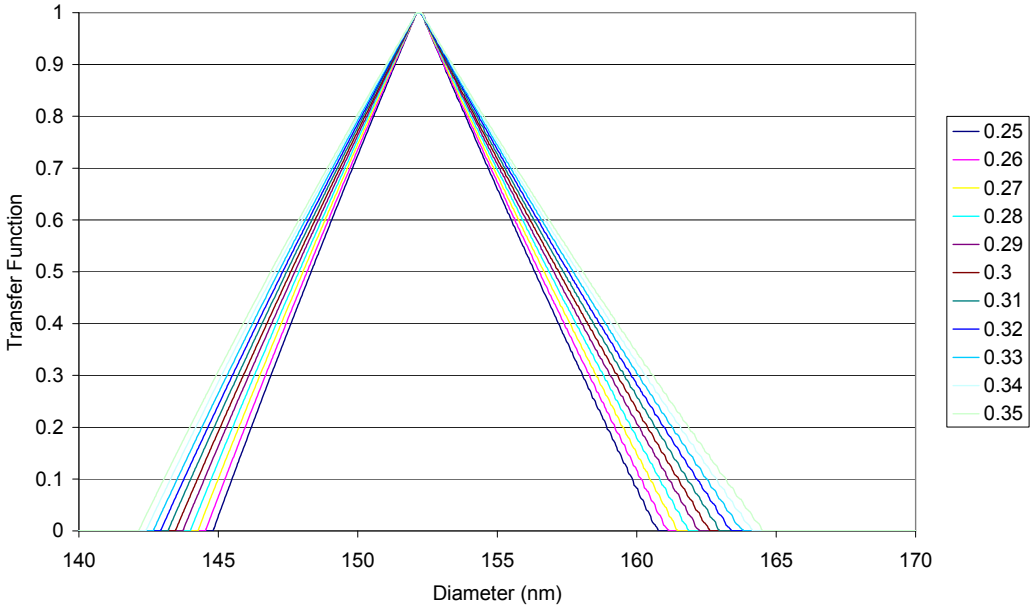

Figure 25: Variation in the DMA transfer function caused by variation of the sample flow rate.

5 Dilution instrumentation

When carrying out laboratory-based experiments, it is desirable to vary the size distribution and number concentration of particles used to challenge the instrumentation under test, in a controlled way. In the case of CPC calibration, control of the number concentration is of particular interest.

Accurate calibration of a diluter is difficult because its performance must be characterised for all particle sizes over the full range of settings, which is time consuming and susceptible to significant measurement issues. Furthermore, each design of diluter has different advantages and drawbacks, meaning that no single design is ideal for all situations. Three of the most common are:

Rotating disc diluter

- Moving parts are prone to scratching, leaks, jamming and failure.
- Near linear variation with rotation speed.
- Constant flow rate.

Bypass diluter

- No moving parts minimising failures.
- Variable pressure drop can affect the performance of either the particle generator or downstream detectors.
- Constant flow rate in a closed system.

Venturi diluter

- No moving parts minimising failures.
- Variable flow, which requires a different experimental configuration to other diluter types.

To examine the application of dilution, its use in CPC calibration is discussed.

5.1 CAST generated soot particles

The configuration used for the soot CPC calibration uses the integrated rotating disc diluter. The level of dilution is controlled by the rotational frequency of the disc (nominal setting 1 to 10), the size and number of chambers on the wheel, and the flow rate of the clean air. During calibration, the absolute number concentration of particles exiting the diluter need not be known, but it is useful to be able to choose the concentration approximately for timesaving purposes. As such, a near linear response is desirable.

During the test calibrations reported earlier, the rotation frequency of the disc was used to control the concentration. As such, the performance of the diluter may readily be determined. Figure 26 illustrates the small but consistent deviation from linear performance observed during the soot calibrations. The repeatability of this deviation indicates that a calibration of this type of diluter is possible.

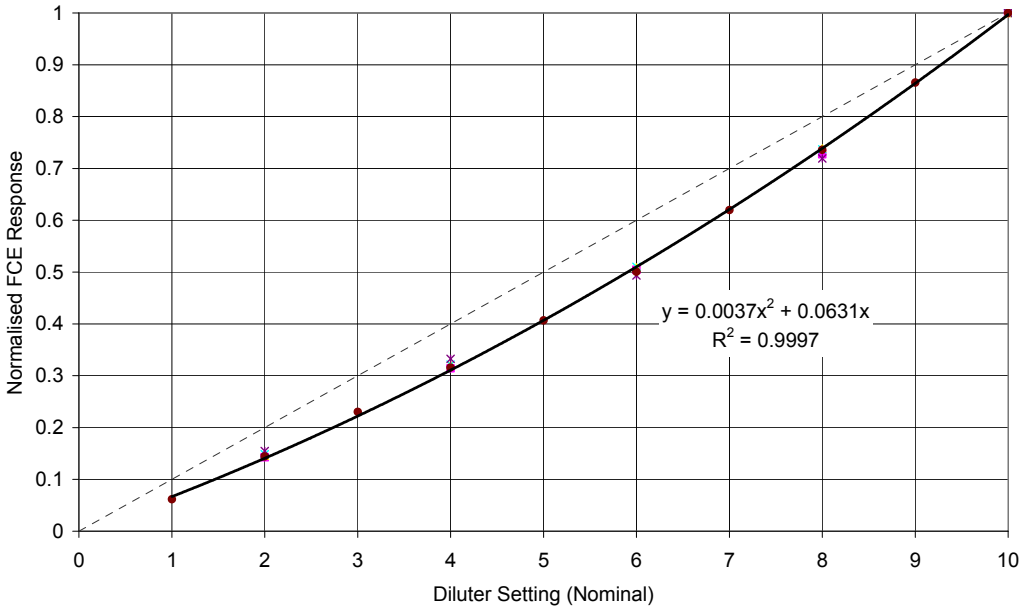

Figure 26: Normalised performance of the CAST rotating disc diluter during trial soot-based CPC calibrations.

5.2 Atomized NaCl

Unlike the CAST generator, CPC calibration using NaCl does not have a built-in means of dilution. Several different dilution systems were tested using both high-volume and low-volume atomizers to find the best combination of stability and prospects for future automation of the calibration procedure. The best combination was found to be the high volume atomizer retrofitted with a Mass Flow Controller (MFC) connected to a Venturi diluter. Initial results shown in Figure 27 show the variation of concentration obtained with different diluter settings. This dilution method appears to provide an acceptable level of control, though further experimental work will be required.

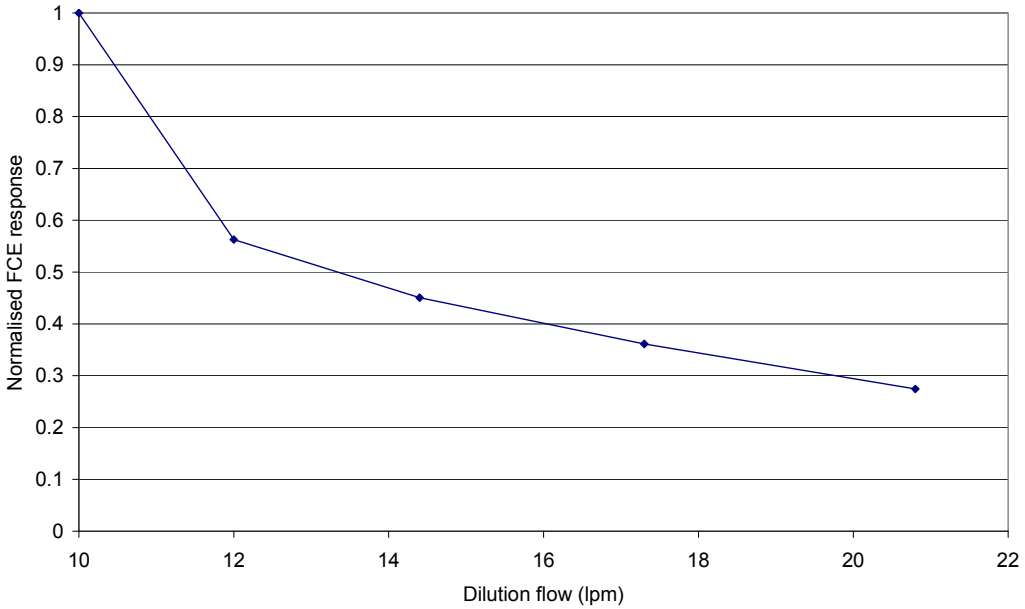

Figure 27: Normalised performance of the modified high volume atomizer diluter during trial NaCl-based CPC calibrations.